Formation of a long-lived hot field reversed configuration by dynamically merging two colliding high-β compact toroids[a)]

H. Y. Guo,[1,b)] M. W. Binderbauer,[1] D. Barnes,[1] S. Putvinski,[1] N. Rostoker,[1] L. Sevier,[1] M. Tuszewski,[1] M. G. Anderson,[1] R. Andow,[1] L. Bonelli,[1] F. Brandi,[2] R. Brown,[1] D. Q. Bui,[1] V. Bystritskii,[1] F. Ceccherini,[1,2] R. Clary,[1] A. H. Cheung,[1] K. D. Conroy,[1] B. H. Deng,[1] S. A. Dettrick,[1] J. D. Douglass,[1] P. Feng,[1] L. Galeotti,[1,2] E. Garate,[1] F. Giammanco,[2] F. J. Glass,[1] O. Gornostaeva,[1] H. Gota,[1] D. Gupta,[1] S. Gupta,[1] J. S. Kinley,[1] K. Knapp,[1] S. Korepanov,[1] M. Hollins,[1] I. Isakov,[1] V. A. Jose,[1] X. L. Li,[1] Y. Luo,[1] P. Marsili,[3] R. Mendoza,[1] M. Meekins,[1] Y. Mok,[1] A. Necas,[1] E. Paganini,[1] F. Pegoraro,[2] R. Pousa-Hijos,[1] S. Primavera,[1] E. Ruskov,[1] A. Qerushi,[1] L. Schmitz,[3] J. H. Schroeder,[1] A. Sibley,[1] A. Smirnov,[1] Y. Song,[1] L. C. Steinhauer,[4] X. Sun,[1] M. C. Thompson,[1] A. D. Van Drie,[1] J. K. Walters,[1] M. D. Wyman,[1] and TAE Team[1]
[1]*Tri Alpha Energy, Inc., P.O. Box 7010, Rancho Santa Margarita, California 92688, USA*
[2]*Department of Physics, University of Pisa, Largo B. Pontecorvo 3, 56127 Pisa, Italy*
[3]*Department of Physics and Astronomy, UCLA, Los Angeles, California 90095-1547, USA*
[4]*Redmond Plasma Physics Laboratory, University of Washington, Redmond, Washington 98052, USA*

(Received 19 November 2010; accepted 7 February 2011; published online 2 May 2011)

A high temperature field reversed configuration (FRC) has been produced in the newly built, world's largest compact toroid (CT) facility, C-2, by colliding and merging two high-β CTs produced using the advanced field-reversed θ-pinch technology. This long-lived, stable merged state exhibits the following key properties: (1) apparent increase in the poloidal flux from the first pass to the final merged state, (2) significantly improved confinement compared to conventional θ-pinch FRCs with flux decay rates approaching classical values in some cases, (3) strong conversion from kinetic energy into thermal energy with total temperature ($T_e + T_i$) exceeding 0.5 keV, predominantly into the ion channel. Detailed modeling using a new 2-D resistive magnetohydrodynamic (MHD) code, LamyRidge, has demonstrated, for the first time, the formation, translation, and merging/reconnection dynamics of such extremely high-β plasmas. [doi:10.1063/1.3574380]

I. INTRODUCTION

The field reversed configuration (FRC) is a compact toroid (CT) with predominantly poloidal fields and zero or small self-generated toroidal fields.[1] The attractions of such a configuration for a potential fusion reactor are its simple geometry for ease of construction and maintenance, a natural unrestricted divertor for facilitating energy extraction and ash removal, and very high β (ratio of plasma to magnetic pressure), i.e., high fusion power density, which is essential for an economic fusion reactor and may also allow use of advanced, aneutronic fuels such as D-He^3 and p-B^{11}.

The traditional method of forming an FRC uses the field-reversed θ-pinch (FRTP) technology, producing hot, high-density plasmas.[2] A variation on this is the *translation-trapping* method in which the plasma created in a θ-pinch "source" is more-or-less immediately ejected out one end into a confinement chamber. The translating plasmoid is then trapped between two strong mirrors at the ends of the chamber.[3–6] Once in the confinement chamber, heating and current drive methods may be applied.[7–9] This separation of source and confinement functions offers key engineering advantages for potential future fusion reactors. FRCs have proved to be extremely robust, resilient to dynamic formation, translation, and violent capture events. Moreover, they show a tendency to assume a preferred plasma state.[5,6] Significant progress has been made in the last decade developing other FRC formation methods: by merging-spheromaks with oppositely directed helicities[10–12] and by driving current with rotating magnetic fields (RMFs),[13–18] which also provides additional stability.[14] Recently, the *collision-merging* technique proposed long ago[19–21] has been developed: θ-pinches at opposite ends of a confinement chamber generate *two* plasmoids and eject them toward each other at high speed; they collide at the center of the chamber and merge to form an FRC. The collision-merging method was shown[22] to produce high temperature FRCs. These FRCs may be the suitable targets for steady-state sustainment, e.g., by neutral beams[7–9] or by RMF,[13–18] as well as magnetized target fusion.[23]

A new, large θ-pinch merging system, C-2, was built to form high-flux, hot FRCs using the collision-merging technique.[24] Stable, long-lived FRCs have been achieved in C-2 with record configuration lifetimes of over 2 ms as compared to traditional θ-pinch-formed and translated FRCs; here, the configuration lifetime is defined as the time interval before the excluded flux signal falls essentially to zero. Plasma diameter is $\sim$1 m, poloidal flux $\phi_p \sim 15$ mWb, $\langle\beta\rangle = 2\mu_o \langle p\rangle / B_e^2 \sim 90\%$ (p is the plasma pressure, B_e is the external magnetic field), electron density $n_e \sim 10^{20}$ m^{-3}, and total

[a)]Paper DI3 1, Bull. Am. Phys. Soc. **55**, 104 (2010).
[b)]Invited speaker.

temperature $T_t = T_i + T_e > 0.5$ keV with $T_i \sim 4.5$ T_e, as inferred from Doppler spectroscopy and multichord, multipulse Thomson scattering measurements. These observations are consistent with simple predictions from the radial force balance. The FRCs are extremely rugged, surviving the violent formation, translation, and merging processes, yet exhibiting strongly enhanced confinement compared to conventional θ-pinches.

In parallel with C-2 experiments, a simulation tool, LamyRidge code, has been developed to better understand the dynamics of formation, translation, and merging/reconnection of these extremely high-β plasmas. LamyRidge is a new 2D resistive magnetohydrodynamic (MHD) code with realistic boundary and initial conditions.

This paper, reporting these new advances, is organized as follows. Section II gives a brief description of the key features of the C-2 merging system. Section III describes the dynamics of the merging, including comparison with modeling results from LamyRidge. Section IV offers evidence that the merged state is an FRC, with detailed internal profiles inferred from various diagnostics, including multichannel, two-color, CO_2/HeNe interferometry, and multichannel, multitime Thomson scattering. Sections V and VI address stability and transport properties, respectively. Finally, Sec. VII presents a summary and conclusions.

II. C-2 FACILITY

Figure 1 is a schematic of the C-2 facility. It consists of a center confinement vessel. Connected to each end of it are θ-pinch formation sections and, beyond them, divertor chambers to control neutral density and impurity contamination. C-2 was built to accommodate ultrahigh vacuum (UHV). The formation sources are standard FRTPs, *albeit* with an advanced pulsed power (PP) formation system. Each formation tube is made of quartz. The confinement chamber is made of stainless steel; it serves as a flux conserver on the timescale of the experiment.

A series of quasi-dc coils are placed along the devices. These produce the basic bias fields in the formation, translation, and confinement sections, as well as a guiding field for directing the end-streaming plasma jets into the remote divertor chambers at the ends. The θ-pinch circuits create a temporary reversed bias of ~ -0.05 T followed by a forward field of $\sim$0.4 T. Field reversal occurs rapidly, ~ 5 μs, driven by multi-GW PP modules. The plasmoids so formed are ejected from the formation sections and expand into the larger diameter confinement chamber. The quasi-dc coils surrounding the confinement chamber produce a forward bias field ~ 0.07 T to control radial expansion and provide the equilibrium external magnetic flux. Separate coils at each end of the confinement chamber can be independently energized for equilibrium shaping control.

In addition, a set of saddle-coil "antennas" are located outside the confinement chamber, four on each side of the midplane. They provide a quasistatic quadrupole field for controlling rotational instabilities. They can also be hooked up to produce the fields symmetric about the midplane or antisymmetric, the latter by driving currents in opposite directions on each side of the midplane.

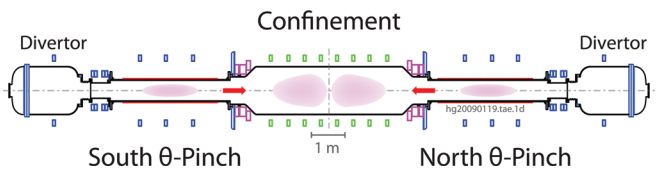

FIG. 1. (Color online) Schematic of the C-2 facility.

III. DYNAMICS OF FRC MERGING

Figure 2 shows a typical time evolution of the excluded flux radius, $r_{\Delta\phi}$, which approximates the separatrix radius, $r_s \sim r_{\Delta\phi}$, to illustrate the dynamics of the θ-pinch merging process. The two individual plasmoids are produced simultaneously and then accelerated out of the respective formation regions at a supersonic speed, $v_Z \sim 250$ km/s and collide near the midplane at $z = 0$. During the collision, the plasmoids compress axially, followed by a rapid radial and axial expansion, before finally merging to form an FRC. The merging process lasts 10's of microseconds, i.e., a few radial Alfvén times. Both radial and axial dynamics of the merging FRC are evidenced by detailed density profile measurements and bolometer-based tomography. As an example, Fig. 3 compares the electron density radial profiles at the midplane for the single-source (only one θ-pinch active) and dual source (merging θ-pinch) FRCs. The density profiles are derived from a six-chord CO_2/HeNe interferometer system[25]

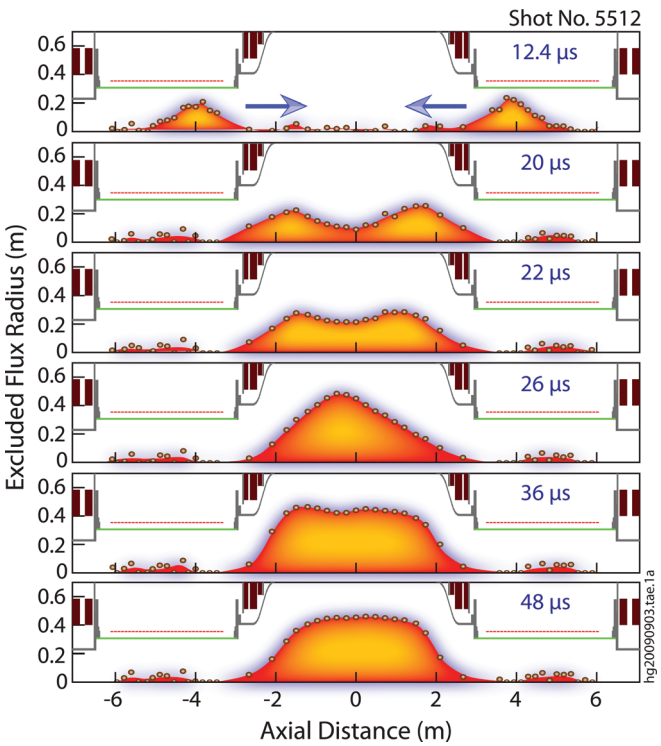

FIG. 2. (Color online) Evolution of the excluded flux radius in C-2 obtained from a series of external diamagnetic loops at the two θ-pinch formation sections and magnetic probes embedded inside the central metal confinement chamber. Time is measured from the instant of synchronized field reversal in the θ pinch sources, and distance z is given relative to the center of the confinement chamber.

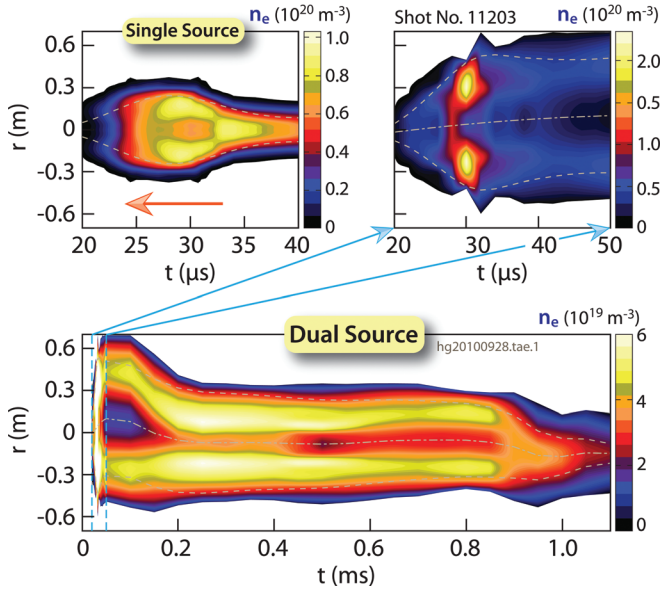

FIG. 3. (Color online) Contours of electron density n_e (r, t) for the single-source (translating) and dual source (collision-merging) FRCs, obtained from a six-channel two-color CO_2/HeNe interferometry located at the midplane of the central confinement chamber using the Abel inversion technique.

by Abel inversion, accounting for the displacement of the FRC axis. The displacement is determined from tomographic reconstruction drawn from an extensive array of both azimuthally and axially distributed bolometers. As can be seen, the single-source plasmoid is relatively narrow and dense with $r_s \sim 0.2$ m and $n_e \sim 10^{20}$ m^{-3}. In dual source operation (θ-pinch merging), the merging plasmoids briefly compress to nearly double the initial value before gradually settling into an equilibrium with $n_e \sim 5\times10^{19}$ m^{-3} while expanding axially. The final merged state exhibits a hollow density profile with peak density near the field null ($R = r_s/\sqrt{2}$), as expected.

The final existence of a merged FRC equilibrium has recently been directly verified by probing the internal magnetic field structure using a multichannel boron-nitride clad magnetic probe at the midplane of the confinement chamber.[26] The probe, however, strongly degraded the performance and overall lifetime of the merged FRC. Interestingly, each of the two translating plasmoids exhibit significant toroidal fields, with opposite signs at each end, i.e., each plasmoid resembles a partially merged spheromaks with opposite helicities at each end. This phenomenon was previously observed in the translation, confinement, and sustainment (TCS) experiment.[5] It appears that most of the toroidal field is annihilated upon merging, leaving little toroidal flux in the merged equilibrium. However, more detailed axial profile measurements are needed to reveal the overall field structure of the merged state.

Magnetic reconnection, recognized in space and astrophysical plasmas,[27,28] is the most fundamental mechanism in self-organization of many low-β magnetic confinement systems such as spheromaks,[29] reversed field pinches (RFPs) (Ref. 30) and other laboratory plasmas.[31–33] Recently, FRC formation by counter-helicity spheromak merging with complete reconnection has been demonstrated both experimentally[10–12] and numerically.[34,35] It was observed that the reconnection rate increased with the initial relative velocity of the two colliding CTs and was highest for counter-helicity merging.[31] The classic 2-D Sweet-Parker (SP) model[36] predicts a reconnection rate too slow to explain many observations in both space and laboratory plasmas.[27] Although many other models have been proposed for faster reconnection, notably Petschek-type models based on standing shock waves,[28] but none of these models has been fully benchmarked in laboratory or space plasmas.

To better understand the formation, translation, and merging processes of colliding FRCs, a new resistive MHD formation code, LamyRidge, has been developed to simulate C-2. In contrast to the 2-D MHD code, MOQUI, which was previously used for FRC formation and translation simulations,[37] LamyRidge is a modern two-dimensional Eulerian code which uses a uniform r,z mesh to represent the poloidal plane and cut-cell boundary conditions to maximize flexibility of boundary conditions. It tracks the dynamics and energetics of the plasma and neutral gas fluids, utilizing realistic experimental geometry and magnetic boundary conditions. A modified system of MHD equations governs the plasma, while a system of fluid equations governs the neutral gas. In addition to friction, the two fluids also exchange density through ionization and charge exchange. The energy equation for the plasma includes radiative energy loss and anisotropic thermal conduction, which is critical in view of the high β of FRCs. An empirical Chodura resistivity is used to model the dissipation of magnetic energy. The present version solves the poloidal MHD (TM polarization) equations with neutral physics and hydrogenic radiation, using the semi-implicit method to permit arbitrary time steps with the large density contrast present in the experimental situation. All other equations are time-implicit, allowing a time step limited only by advection, which is treated by a predictor-corrector method. Iterative methods are used to solve for the flux function, velocity components, and temperature. The propagation of the compression wave during the formation is modeled by a modern shock capturing method (SMART). Figure 4 shows a simulation of the same discharge shown in Fig. 2. As can be seen, it well reproduces the observed formation, translation, and merging dynamics of the collision-merged FRC. In particular, the merging of two individual plasmoids into a single entity is evidenced by the closed poloidal field structure in the merged equilibrium, e.g., at 48 μs.

IV. POLOIDAL FLUX INCREAE AND RETHERMALIZATION DURING MERGING

What is truly remarkable is that the poloidal flux, ϕ_p appears to increase significantly during the merging process. Figure 5 shows the time evolution of single plasmoids produced in separate discharges, one produced by the south pinch and one by the north pinch, as well as the merged FRC with both pinches fired simultaneously, under the same operating conditions. The data were taken at the midplane of the confinement chamber. Note that the single plasmoids pass

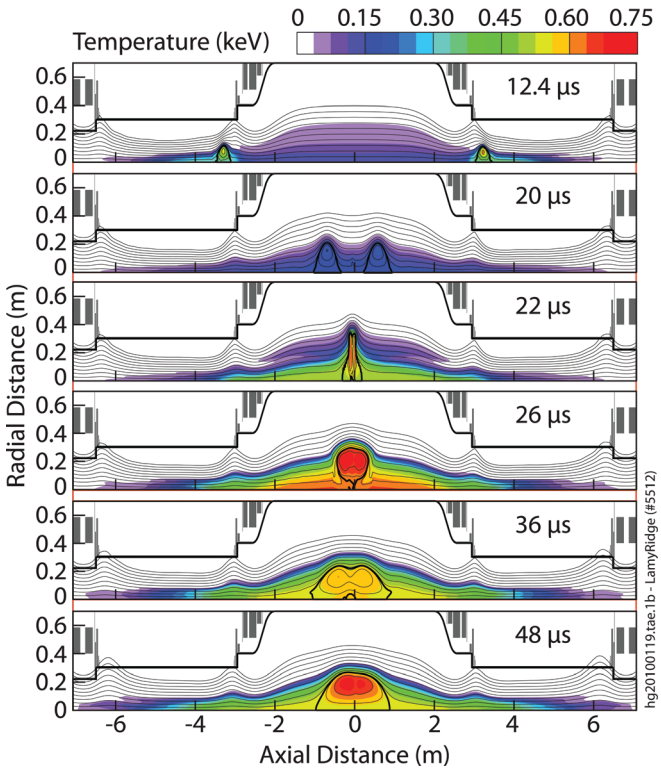

FIG. 4. (Color online) Simulation of FRC formation, translation, and merging dynamics for the same shot as shown in Fig. 2, i.e., #5512, showing time histories of both magnetic flux and temperature predicted by the 2-D resistive MHD code, LamyRidge. The magnetic reconnection induced by collision is clearly demonstrated by the evolution of the flux contours.

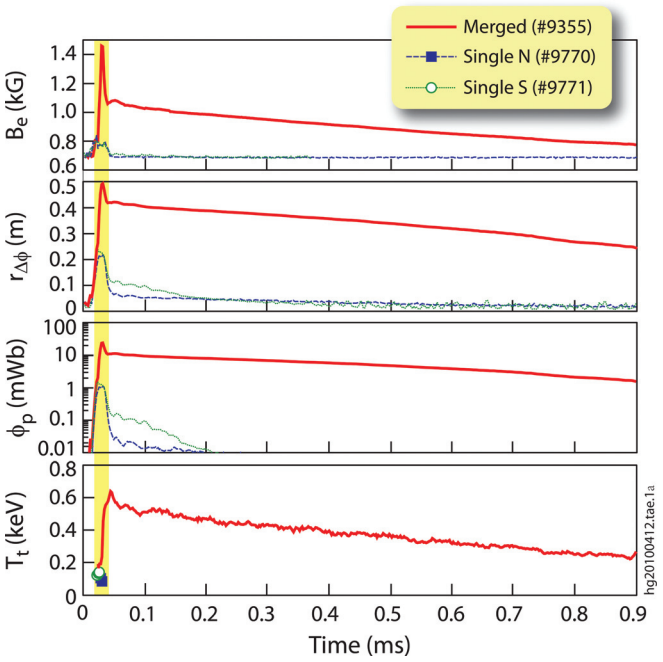

FIG. 5. (Color online) Comparison of the initial translated CTs and the resultant merged FRC, showing time traces of the external poloidal field, B_e, the excluded flux radius, $r_{\Delta\phi}$, the poloidal flux, ϕ_p, and the total temperature, $T_t = T_i + T_e$, derived from radial pressure balance, for individual CTs produced by θ-pinches on the north side and the south side, respectively, and the result from merging individual CTs formed under identical conditions. Note that the two single CTs were not captured by the end mirrors due to their high translation speeds. Merging occurs around 30 μs, as indicated.

through the confinement chamber without being captured because of their high translation speed and the insufficient magnetic mirrors at the ends of the chamber. The poloidal flux is estimated as

$$\phi_p = 0.31\pi B_e r_s^3 / r_c, \tag{1}$$

assuming a rigid rotor (RR) profile, which was consistent with internal probe measurements for translated CTs.[5] Here, r_c is the radius of the metal confinement chamber, which acts as a flux conserver. Clearly, the individual plasmoids, as they first pass (*fp*) the midplane, have relatively small poloidal fluxes, while the merged FRC exhibits a substantial increase in ϕ_p, with a flux amplification factor exceeding 10 as a result of the merging. This factor is defined as the ratio of the poloidal flux of the merged FRC to the average poloidal flux of the individual plasmoids during their *fp* through the midplane, i.e., $2\phi_M/(\phi_N^{fp} + \phi_S^{fp})$. Merging is complete by ~40 μs, as highlighted in Fig. 5. Note that the RR approximation of ϕ_p may be inaccurate for the highly dynamical translating plasmoids.

While the details of the merging process are unclear, the final state has very high β. Evidently, it is not a Taylor state, which is force-free with $\beta = 0$ (Ref. 30), objects which have been observed in astrophysical plasmas and low-β laboratory plasmas. Although more general relaxation principles have been advanced,[38–40] none has yet been verified by experiment. Thus, the underlying relaxation principle in these high-β plasmas remains unclear.

Strong rethermalization occurs during the merging process, as shown in Fig. 5. As can be seen, the total temperature, $T_t = T_i + T_e \leq 100$ eV for the single plasmoids, exceeds 600 eV in the merged FRC, in agreement with the LamyRidge code prediction (Fig. 4). Here, T_t derives from the radial pressure balance, i.e.,

$$T_t = B_e^2/(2\mu_0 k_B n_m), \tag{2}$$

where k_B is Boltzmann's constant and n_m is the peak electron density at the field null. The latter is extracted from $\bar{n}$, the line average density from CO_2/HeNe interferometry, using $n_m = \bar{n}/\langle\beta\rangle$, with the average β from axial force balance, i.e.,

$$\langle\beta\rangle = 1 - {}^1\!/_2 x_s^2, \tag{3}$$

where $x_s = r_s/r_c$ is the ratio of the separatrix radius to the flux conserver radius. $\langle\beta\rangle \approx 0.9$ for typical merged FRCs on C-2. Rethermalization also occurs in translation-trapping formation,[3–6] but with a smaller fraction of the translation energy being converted to heat.

Figure 6 shows the first electron temperature profile measurements (still being investigated in detail) for a translating plasmoid (single-source) and a collision-merged FRC, obtained from a nine-chord Thomson scattering diagnostic,[41] using a multipulse ruby laser. As can be seen, $T_e \sim T_t/2 \leq 50$ eV for the translating plasmoid, while rising above 100 eV for the collision-merged FRCs.

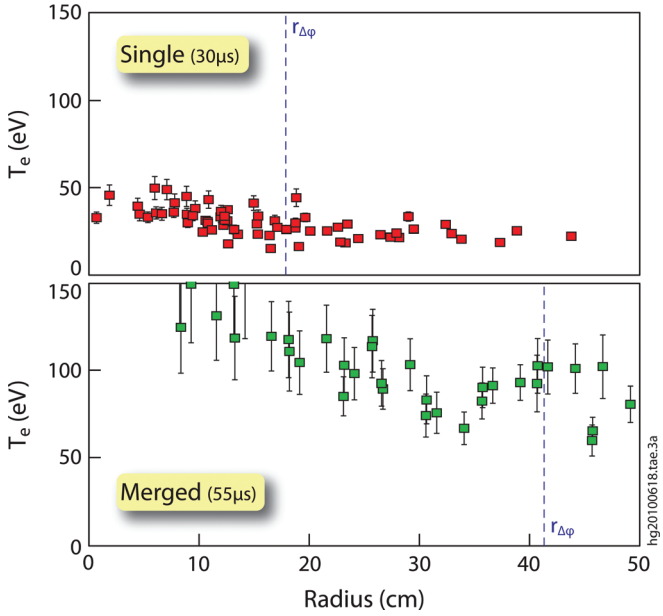

FIG. 6. (Color online) Comparison of radial electron temperature profiles, $T_e(r)$, obtained from a nine-chord Thomson scattering system for individual plasmoids and merged FRCs.

Strong ion heating occurs during the merging, as observed in FRCs formed by counter-helicity spheromak merging,[10–12,42] demonstrating direct conversion of magnetic energy into ion thermal energy arising from the annihilation of toroidal fields. Figure 7 shows ion temperatures obtained from ion Doppler broadening spectroscopy[43] using O–V (O^{4+}) line emissions at 297.1 nm. All the ion Doppler measurements were taken during the quiescent decay phase of merged FRC and well after the dynamic phase of CT merging. This minimizes the effects of magnetic reconnection on the ion temperature measurements, which may be present during the merging process. Clearly, Doppler spectroscopy shows a substantial increase in ion energy during the merging process, with $T_i \sim 4.5T_e$ in collision-merged FRCs, as shown in Fig. 7, consistent with the total temperatures derived from the radial pressure balance, $T_t^p \sim 1.2T_i \sim 5.5T_e$. Note that for typical density 5×10^{19} m^{-3}, the thermalization time for Oxygen–V ions ($Z = 4$) with background Deuterium ions is below 30 μs for the temperature range in Fig. 7, based on the Spitz energy transfer time:[44]

$$\tau_z(ms) \approx \frac{0.1 m_z(amu) T_i(keV)_i^{3/2}}{n_i(10^{20} m^{-3}) Z^2}. \quad (4)$$

This is significantly smaller than the FRC thermal energy confinement time, i.e., 400 μs, for typical merged FRCs. Also note that the data shown in Fig. 7 were obtained with internal magnetic probes present in the plasma, which are lower than usual merged FRCs due to probe perturbation, as mentioned in Sec. III.

Both poloidal flux and total temperature of the collision-merged FRCs depend strongly on the translation speed of the colliding plasmoids, favoring fast translation, as shown in Fig. 8. The C-2 design allows flexible formation schemes, ranging from fully *dynamic* to *static*. *Dynamic* formation achieves the fastest translation speed by sequentially energizing the individual coils in the θ-pinches from back to front; this rapidly accelerates the plasmoids out of their respective sources. By contrast, in *static* formation, only the far end coils are energized slightly early to gently nudge the plasmoids into the confinement chamber.

As aforementioned, despite the strong dynamics, preliminary measurements from the internal probe reveal the presence of significant and opposed toroidal fields at the front and rear of each translating plasmoid. Such axially antisymmetric toroidal fields may arise from poloidally sheared toroidal electron flow,[45] or from the translation itself, as in a

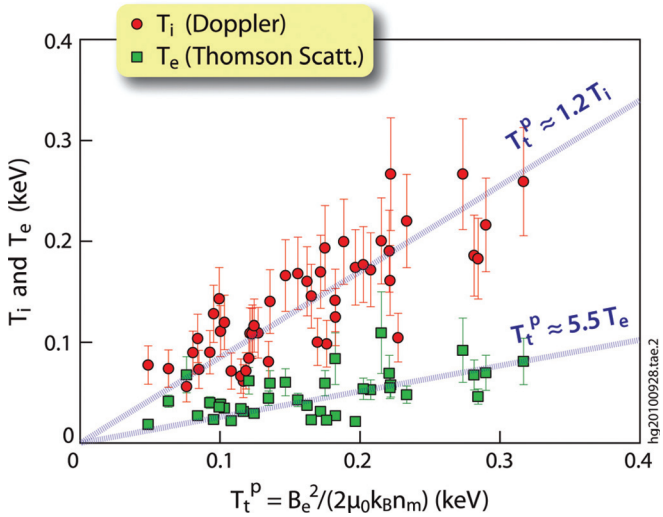

FIG. 7. (Color online) Ion temperature, T_i, from Doppler spectroscopy and electron temperature, T_e, from Thomson scattering vs total temperature, T_t, derived from radial pressure balance, in merged FRCs.

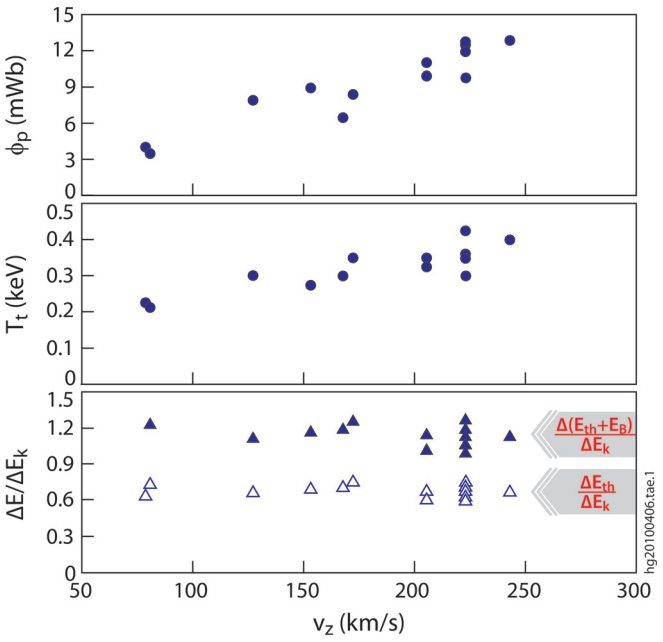

FIG. 8. (Color online) Effect of dynamic translation speed. The data are obtained right after merging ($\sim$ 40 μs) of the FRCs from a series of reproducible and well-controlled discharges with the same magnetic configurations and gas fuelling rates. The translation speed is varied by energizing the θ-pinch coils at various different times during the initial formation process.

conical θ-pinch.[46] Simulations by including the Hall term reproduce this.[37] Increasing the translation speed might increase the toroidal field generation, and thus, the subsequent flux-conversion from toroidal to poloidal flux.

The plasma temperature of the merged state is dictated by the conservation of the total energy, including kinetic energy of the translated FRCs $E_k = {}^1\!/_2 N m_i v_z^2$, thermal energy $E_{\text{th}} = {}^3\!/_2 N k_B T_t$, and *poloidal* magnetic energy $E_B = N k_B T_t$[4]. Here, N is the total number of ions and m_i is the ion mass. Note that the E_B estimate includes the magnetic energy *outside* the FRC, because the presence of the flux-excluding plasma compresses the external field. Assuming conservation of particles from before to after merging leads to the following simple relationship,

$$\frac{5}{2} k_B T_t + \frac{1}{2} m_i v_z^2 = \text{constant}. \tag{5}$$

As shown in Fig. 8, over 60% of the kinetic energy, E_k, is converted into plasma thermal energy, E_{th}, upon merging with the rest going into magnetic energy. The ratio of the change in total FRC internal energy to the change in kinetic energy, $(\Delta E_{th} + \Delta E_B)/\Delta E_k$, appears to slightly exceed unity: this may be attributed to loss of lower energy particles during the merging or uncertainties in the translation speed. However, this may also arise from direct conversion of *toroidal* magnetic energy stored in the toroidal fields that are present in the translating plasmoids, as observed in merging-spheromak formation.

V. STABILITY

One of the most important issues for an FRC is its stability to low-n MHD modes, since Finite-Larmor-Radius (FLR) effects suppress higher-n modes.[1] The $n=1$ tilt mode, which appears as a primarily axial shift in elongated FRCs, is unstable according to MHD theory with a fast growth rate, but it is not observed in present kinetic FRCs. The stability is primarily attributed to the highly kinetic nature of FRCs with various contributing mechanisms such as two-fluid minimum-energy state,[38–40] sheared flow,[11] and small but finite toroidal fields in FRCs.[6,15,47] Recent nonlinear kinetic simulations have exhibited in some cases the nonlinear saturation of the tilt instability without disrupting the FRC.[48,49] The global instability clearly observed experimentally is the $n=2$ rotational mode, driven by the centrifugal effect of plasma rotation. The $n=2$ mode is disruptive in θ-pinch-formed FRCs, but it is readily stabilized by applying a static multipole field.[50] Multipole stabilization requires that the average magnetic pressure from the multipole fields counterbalance the centrifugal force, with the stability criterion[51]

$$\frac{B_m^2}{\mu_0} \geq \frac{{}^1\!/_4 \langle n_i m_i \rangle \Omega_i^2 r_s^2}{(\ell - 1)}, \tag{6}$$

where B_m is the multipole field strength, Ω_i is the ion rotation frequency, and 2ℓ is the order of the multipole field ($\ell = 2$ for quadrupoles). Recently, rotating magnetic fields (the rotating analogy of static multipoles) also provided stabilization of rotational instability.[14]

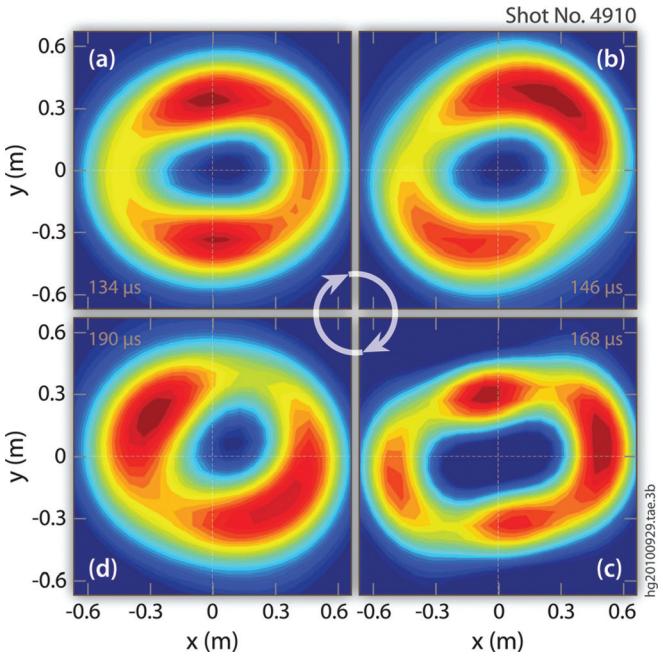

FIG. 9. (Color online) Tomographic reconstruction of bremsstrahlung radiation in the FRC with $n=2$ mode, obtained from a 60-chords visible tomography system. Frame (a) was obtained at the onset of the $n=2$ mode, and frames (b)–(d) during half cycle of the $n=2$ mode, rotating in the ion diamagnetic direction.

The $n=2$ mode also develops in the collision-merged FRCs in C-2, especially in lower density, hotter FRCs; however, it is usually not disruptive, tending rather to saturate. The $n=2$ mode appears in tomography as an elliptical distortion of the FRC cross section, as shown in Fig. 9, for a discharge without the application of stabilizing quadrupole field. The mode rotation is in the ion diamagnetic direction with the frequency similar to the ion diamagnetic frequency, i.e., $f_{n=2} \sim \Omega_i^* / 2\pi \sim 10$ kHz for typical FRCs in C-2. This is consistent with bolometric radiation reconstructions. Further information comes from the Mirnov B_θ probe arrays inserted on two toroidal planes ($z = \text{const.}$) distributed along θ. These measurements showed an axially rigid rotation of the $n=2$ mode structure. The $n=1$ rotational mode (wobble) was also observed by the Mirnov probes, but at a much lower frequency.

The evolution of the density profile with the $n=2$ mode has been obtained from interferometry by simultaneously fitting the line-integrated density measurements from each individual channel. The $n=2$ mode is modeled as an elliptical distortion of the FRC cross section, assuming a modification of the RR profile,

$$n = n_m \operatorname{sech}^2 \left[K_{RR} \left(\frac{a^2}{a_s^2} + \frac{b^2}{b_s^2} - 1 \right) \right], \tag{7}$$

where K_{RR} is the RR profile parameter, a and b represent the short and long axes of each ellipse, and a_s, b_s are their separatrix values; the effective separatrix $r_s = \sqrt{a_s b_s}$. Figure 10(a) shows the integrated density measurements, $\int n d\ell$, and the modeled results during a half cycle of the $n=2$ rotation. Clearly, the modified RR model (dashed line) reproduces the

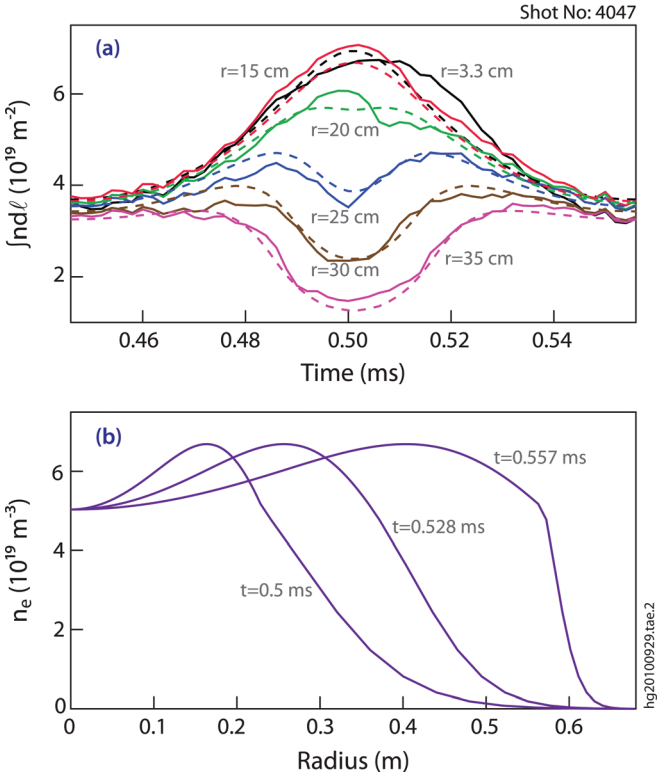

FIG. 10. (Color online) (a) Line-integrated density measurements, $\int ndl$, from separate channels at different impact parameters of the CO_2/HeNe interferometer, located at the center of the confinement chamber ($z=0$) and fitted results for shot #4047; (b) density profiles during the $n=2$ rotation at ~ 0.5 ms, obtained from the modified RR model.

observations on all channels. Figure 10(b) shows the time-resolved density profile predicted by the model. Note that steep edge gradients appear during the rotation. This correlates with increased fluctuation levels at the edge, as discussed later, which may thus enhance the radial transport rate.

Density fluctuations arising from the $n=2$ rotational mode have been measured, for the first time in an FRC, using the newly developed heterodyne six-channel reflectometry, based on the Doppler backscattering, by launching the microwave beam oblique to the magnetic surface. Figure 11 shows the density fluctuation spectra from reflectometry and simultaneous line-integrated density from CO_2/HeNe interferometry. The Doppler shift is asymmetric, consistent with a mixed $n=1$ and $n=2$ oscillation with a net toroidal rotation. For the example in Fig. 11, the Doppler shift frequency $\langle \Delta f_D \rangle \sim 1$MHz and $k_\theta \sim 4$ cm^{-1}, thus, the toroidal rotation velocity, $\langle V_\theta \rangle = 2\pi \langle \Delta f_D \rangle / k_\theta \sim 16$km/s. This is consistent with results from Mirnov probes and bremsstrahlung/bolometer tomography.

In order to further improve stability against the $n=2$ mode, quasistatic quadrupole fields are routinely applied in C-2 by configuring the saddle coils outside the confinement chamber as standard quadrupole. For typical conditions with $n_i \sim 5\times10^{19}$ m^{-3}, $r_s \sim 0.35$ m, and $\Omega_i \sim 2\pi f_{n=2} = 6.3\times10^4$ rad/s, the predicted field strength required for quadrupole stabilization, according to Eq. (6), is $B_{\text{quad}} \sim 50$ G at the separatrix. Figure 12 compares cases with and without quadrupole fields, obtained under similar operating conditions; here, the vacuum quadrupole field at the separatrix ($r_s = 35$ cm) is $B_{\text{quad}} = 50$ G, which satisfies the stability criterion. The $n=2$ mode appears as amplitude oscillations of the line-integrated density, $\int ndl$. Clearly, quadrupole field significantly delays the onset of the instability, significantly extending the initial higher performance phase from ~ 0.2 to ~ 0.9 ms, as indicated by slower decay in B_e and $r_{\Delta\varphi}$. It is worth nothing that multipoles also provide an effective means of stabilizing the instability in traditional θ-pinch FRCs, but without improving confinement.[1] However, at the late time, i.e., ~ 0.9 ms, stability is lost because $r_s \sim r_{\Delta\varphi}$ has shrunk considerably and B_{quad} at the separatrix has fallen

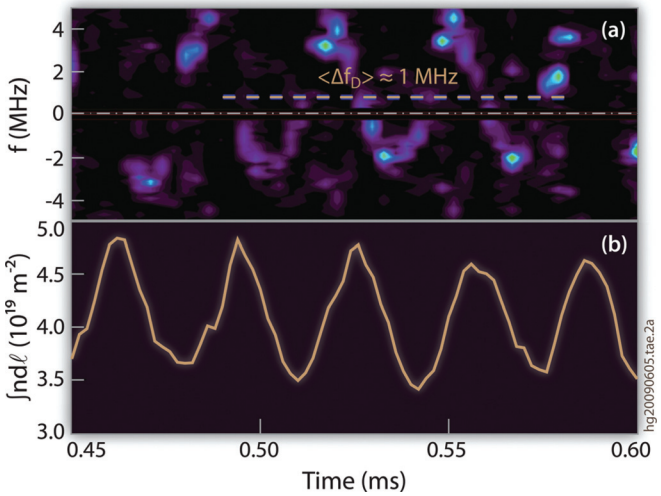

FIG. 11. (Color online) (a) Fluctuation spectra at the edge, obtained from the reflectometer; (b) line-integrated density, $\int ndl$, obtained from the interferometer with a line of sight near the center of the FRC.

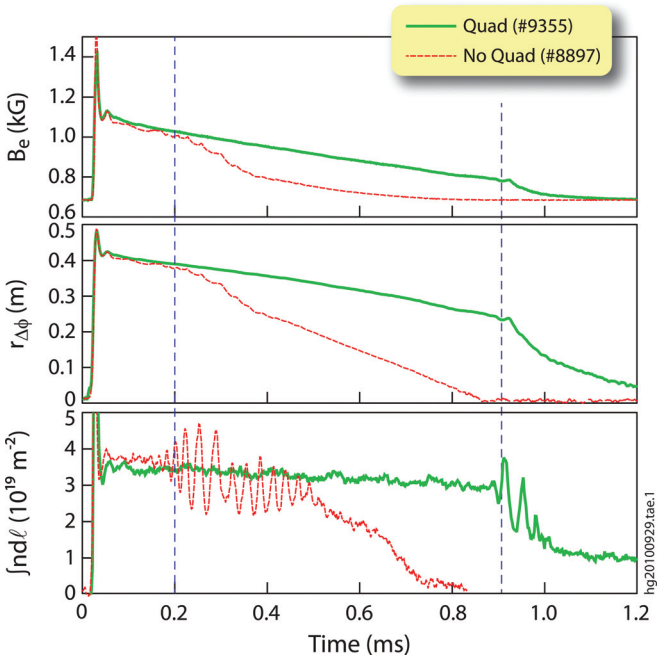

FIG. 12. (Color online) Effect of quadrupole stabilization against the $n=2$ mode, which can be clearly seen from the amplitude oscillations on the line-integrated density, $\int ndl$. Onset of the $n=2$ modes also indicated.

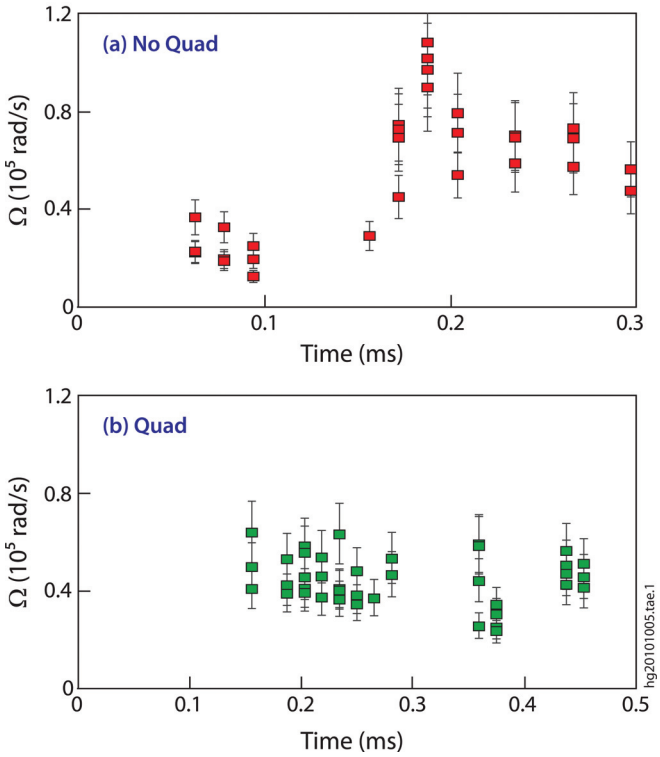

FIG. 13. (Color online) Time evolution of plasma rotation frequency, Ω, with and without quadrupole stabilization.

below the stability requirement. Applying a stronger quadrupole was found to compromise the initial FRC performance, possibly because of field-line opening by the radial component of the quadrupole field. An "odd parity" quadrupole (antisymmetric about the midplane) was tested and also found to stabilize the instability, *albeit* requiring higher field strength than the standard "even parity" (symmetric) quadrupole.

Figure 13 shows the toroidal plasma rotation frequencies of collision-merged FRCs in C-2 obtained from reflectometry for the discharges with and without quadrupole stabilization. Without quadrupole fields, Fig. 13(a), the plasma spins up during the initial quiescent phase, with rotation frequency, Ω, reaching $\sim 1\times10^5$ rad/s at the onset of the $n=2$ mode, i.e., at ~ 0.2 ms, see Fig. 12. After that Ω appears to decrease as the $n=2$ mode saturates. By contrast, with quadrupole stabilization, Fig. 13(b), the initial rotation appears to be suppressed with $\Omega < 5\times10^4$ rad/s. This is consistent with the observations from FRX-C.[52] Note, however, that multipoles usually do not suppress the plasma rotation in most θ-pinch FRCs, but merely mitigate the growth of the $n=2$ mode.[1]

VI. CONFINEMENT AND TRANSPORT

The FRC is predominantly a diamagnetic entity supported by bulk currents flowing *across* the poloidal field, i.e., currents arising from drifts. Hence, both the quality of confinement and the effectiveness of current drive are ultimately limited by cross-field transport, which is well known to be anomalous (nonclassical) in magnetic confinement systems. Little has been established quantitatively about FRC transport other than what can be characterized by empirical expressions. On the other hand, it is well established that the loss of particles at the separatrix and the decay of the poloidal flux (or equivalently, the plasma current) are intimately connected, a consequence of high β. Further, the bulk transport of energy appears to be convective and so linked intimately to the loss of particles.[53] Thus, the general character of the transport is captured by the poloidal flux decay as a resistive diffusion process. The diffusivity, $D_\perp$, follows from the flux decay time τ_ϕ as

$$D_\perp \equiv \eta_\perp/\mu_0 = a^2/\tau_\phi, \tag{8}$$

where $a = r_s - R \approx r_s/4$ is nominal minor radius, taken to be the distance between the field null (R) and the separatrix (r_s).

Figure 14(a) shows the flux confinement times of the FRCs formed by collision-merging ("M") in C-2 and those formed by translation-trapping ("T"). These are compared to the empirical LSX-scaling obtained from the large s experiment (LSX) for θ-pinch-formed FRCs,[2]

$$\tau_\phi^{\mathrm{LSX}} = 6.52\times10^{-5}\rho_L^{-1.07}x_s^{0.5}r_s^{2.14}, \tag{9}$$

where ρ_L is the ion Larmor radius based on the external magnetic field. The LSX scaling is also in accordance with the results from the early CT merging experiment with conical

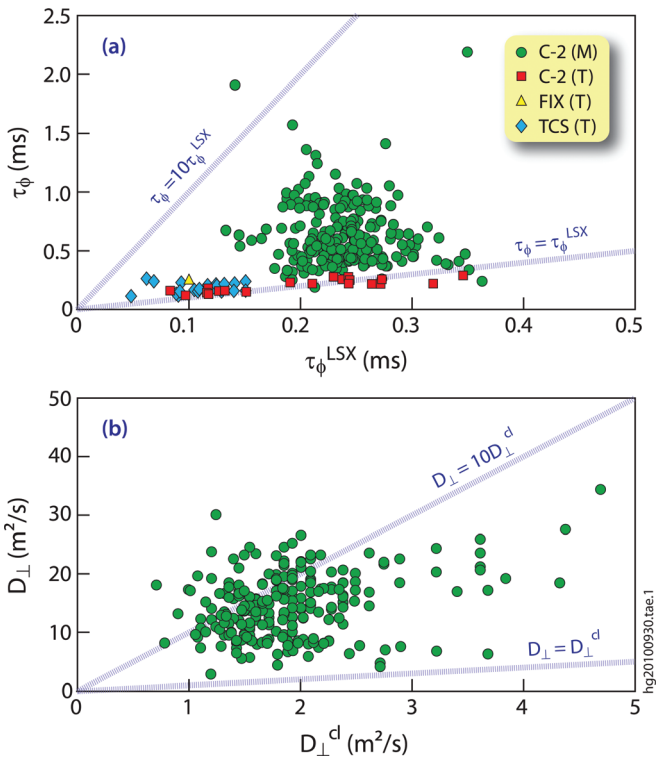

FIG. 14. (Color online) (a) Magnetic flux confinement time of merged FRCs in C-2, τ_φ, vs the LSX scaling for conventional θ-pinch-formed FRCs, τ_ϕ^{LSX}, along with the results from recent FRC translation experiments, FIX[3], TCS[6], as well as those obtained on C-2 during the initial start-up phase with only one single θ-pinch formation source attached to the central confinement chamber and a strong magnetic mirror plug at the downstream end to capture the translated FRCs; (b) diffusivities, $D_\perp$, derived from τ_φ, vs classical diffusivities, $D_\perp^{cl}$, for the well-centered merged FRCs in C-2.

conical θ-pinches.[19–21] The translation-trapping formation examples ("T") are from FIX [FRC Injection eXperiment,[3] TCS (Ref. 6)], as well as early C-2 experiments. The early C-2 results were obtained using a single θ-pinch source; the downstream magnetic mirror was strong enough to trap the rapidly translating plasmoid. FRCs formed by translation-trapping exhibit a confinement comparable to but up to a factor of 2 better than LSX scaling. By contrast, many merged FRCs on C-2 exhibit a remarkable improvement in confinement up to ten times LSX scaling. Note that instrumental errors in the magnetic measurements are only about ~2%; larger data scatters in the figure largely reflect shot-to-shot variations in experimental conditions.

Figure 14(b) plots the transport rates for collision-merged FRCs, inferred using Eq. (8), compared to the classical diffusivity,[54]

$$D_{\perp}^{\mathrm{cl}} = 2D_{//}^{\mathrm{cl}} \approx 0.45 Z_{\mathrm{eff}} T_t [\mathrm{keV}]^{-3/2} \tag{10}$$

assuming $Z_{\mathrm{eff}} = 1$ and $T_t / T_e = 5.5$ (the latter based on Thomson scattering, Doppler spectroscopy, and magnetic measurements, see Fig. 7). While there is no clear trend, the best collision-merged FRCs exhibit near-classical confinement. Indeed, the transport may be even closer to the classical, if plasma impurities ($Z_{\mathrm{eff}} > 1$) are taken into account. More detailed data and a broader parameter space are needed to develop a physics-based transport understanding.

VII. SUMMARY AND CONCLUSIONS

High-temperature, stable FRCs have been produced in a new compact toroid research facility, C-2, employing the collision-merging formation method, i.e., merging of two colliding, highly supersonic, high-β plasmoids. These FRCs achieved record lifetimes of the diamagnetism, some exceeding 2 ms. Poloidal flux increases during the merging, compared to the first pass, with a poloidal flux-increase factor exceeding 10. Most of the kinetic energy of the plasmoids is converted into the thermal energy during the merging, predominantly going into the ion channel: before merging $T_i \sim T_e \sim 30$ eV and after merging $T_i \sim 4.5 T_e$ with $T_e \sim 100$ eV. Both the temperature and poloidal flux of merged FRC strongly depend on the translation speed of the individual plasmoids, favoring higher speeds. The dynamics of FRC formation, translation, and merging/reconnection processes are reproduced by a newly developed 2-D resistive magneto-hydrodynamic code, LamyRidge.

The collision-merged FRCs in C-2 exhibit a spectacular improvement in flux confinement compared to the FRCs formed by the original θ-pinch method, with flux transport rates approaching classical values in some cases. The ability to generate these well-confined, long-lived, high-β plasmas, using collision-merging via magnetic reconnection, should have significant implications for fusion energy research and basic plasma physics.

ACKNOWLEDGMENTS

We thank our shareholders for their support and trust and the rest of the TAE staff for their dedication, excellent work, and extra efforts. A debt of gratitude is also due to John Slough for his advice during the initial design of C-2.

[1] M. Tuszewski, Nucl. Fusion **28**, 2033 (1988).
[2] A. L. Hoffman and J. T. Slough, Nucl. Fusion **33**, 27 (1993).
[3] H. Himura, S. Okada, S. Sugimoto, and S. Goto, Phys. Plasmas **2**, 191 (1995); M. Inomoto, private communications (2002).
[4] D. J. Rej, W. T. Armstrong, R. E. Chrien, P. L. Klingner, R. K. Linford, K. F. McKenna, E. G. Sherwood, R. E. Siemon, M. Tuszewski, and R. D. Milro, Phys. Fluids **29**, 852 (1986).
[5] H. Y. Guo, A. L. Hoffman, K. E. Miller, and L. C. Steinhauer, Phys. Rev. Lett. **92**, 245001 (2004).
[6] H. Y. Guo, A. L. Hoffman, L. C. Steinhauer, and K. E. Miller, Phys. Rev. Lett. **95**, 175001 (2005).
[7] T. Asai, Y. Suzuki, T. Yoneda, F. Kodera, M. Okubo, S. Okada, and S. Goto, Phys. Plasmas **7**, 2294 (2000).
[8] S. Okada, T. Asai, F. Kodera, K. Kitano, Y. Suzuki, K. Yamanaka, T. Kanki, M. Inomoto, S. Yoshimura, M. Okubo, S. Sugimoto, S. Ohi, and S. Goto, Nucl. Fusion **41**, 625 (2001).
[9] M. Inomoto, T. Asai, and S. Okada, Nucl. Fusion **48**, 035013 (2008).
[10] Y. Ono, M. Inomoto, Y. Ueda, T. Matsuyama, and T. Okazaki, Nucl. Fusion **39**, 2001 (1999).
[11] Y. Ono, T. Matsuyama, K. Umeda, and E. Kawamori, Nucl. Fusion **43**, 649 (2003).
[12] C. D. Cothran, A. Falk, A. Fefferman, M. Landreman, and M. R. Brown, Phys. Plasmas **10**, 1748 (2003).
[13] I. R. Jones, Phys. Plasmas **6**, 1950 (1999).
[14] H. Y. Guo, A. L. Hoffman, R. D. Milroy, K. E. Miller, and G. R. Votroubek, Phys. Rev. Lett. **94**, 185001 (2005).
[15] H. Y. Guo, A. L. Hoffman, L. C. Steinhauer, K. E. Miller, and R. D. Milroy, Phys. Rev. Lett. **97**, 235002 (2006).
[16] M. Inomoto, K. Kitano, and S. Okada, Phys. Rev. Lett. **99**, 175003 (2007).
[17] S. A. Cohen, B. Berlinger, C. Brunkhorst, A. Brooks, N. Ferraro, D. P. Lundberg, A. Roach, and A. H. Glasser, Phys. Rev. Lett. **98**, 145002 (2007).
[18] X. Yang, Y. Petrov, and T. S. Huang, Phys. Rev. Lett. **102**, 255004 (2009).
[19] D. R. Wells, Phys. Fluids **9**, 1010 (1966).
[20] D. R. Wells, J. Davidson, L. G. Phadke, J. G. Hirschberg, P. E. Ziajka, and J. Tunstall, Phys. Rev. Lett. **41**, 166 (1978).
[21] D. R. Wells, P. E. Ziajka, and J. L. Tunstall, Fusion Technol. **9**, 83 (1986).
[22] G. Votroubek, J. Slough, S. Andreason, C. Pihl, J. Fusion Energy **27**, 123 (2008).
[23] R. C. Kirkpatrick, I.R. Lindemuth, M.S. Ward, Fusion Technol. **27**, 201 (1995).
[24] M. Binderbauer, H. Y. Guo, M. Tuszewski, S. Putvinski, L. Sevier, D. Barnes, N. Rostoker, M. G. Anderson, R. Andow, L. Bonelli, F. Brandi, R. Brown, D. Q. Bui, V. Bystritskii, F. Ceccherini, R. Clary, A. H. Cheung, K. D. Conroy, B. H. Deng, S. A. Dettrick, J. D. Douglass, P. Feng, L. Galeotti, E. Garate, F. Giammanco, F. J. Glass, O. Gornostaeva, H. Gota, D. Gupta, S. Gupta, J. S. Kinley, K. Knapp, S. Korepanov, M. Hollins, I. Isakov, V. A. Jose, X. L. Li, Y. Luo, P. Marsili, R. Mendoza, M. Meekins, Y. Mok, A. Necas, E. Paganini, F. Pegoraro, R. Pousa-Hijos, S. Primavera, E. Ruskov, A. Qerushi, L. Schmitz, J. H. Schroeder, A. Sibley, A. Smirnov, Y. Song, X. Sun, M. C. Thompson, A. D. Van Drie, J. K. Walters, M. D. Wyman, and the TAE Team, Phys. Rev. Lett. **105**, 045003 (2010).
[25] O. Gornostaeva, B. H. Deng, E. Garate, H. Gota, J. Kinley, J. Schroeder, and M. Tuszewski, Rev. Sci. Instrum. **81**, 10D516 (2010).
[26] H. Gota, K. Knapp, B. Deng, M. Thompson, M. Tuszewski, A. Van Drie, and TAE Team, Bull. Am. Phys. Soc. **55**, GP9.00101 (2010).
[27] M. Yamada, R. M. Kulsrud, and H. Ji, Rev. Mod. Phys., **82**, 603 (2010).
[28] E. Priest, T. Forbes, *Magnetic Reconnection* (Cambridge University Press, Cambridge, 2006).
[29] P. M. Bellan, *Spheromaks* (Imperial College Press, London, 2000).
[30] J. B. Taylor, Phys. Rev. Lett. **33**, 1139 (1974).
[31] M. Yamada, Y. Ono, A. Hayakawa, M. Katsurai, and F. W. Perkins, Phys. Rev. Lett. **65**, 721 (1990).
[32] M. R. Brown, Phys. Plasmas **6**, 1717 (1999).
[33] T. P. Intrator, X. Sun, G. Lapenta, L. Dorf, and I. Furno, Nature Phys. **5**, 521 (2009).
[34] T.-H. Watanabe, T. Sato, and T. Hayashi, Phys. Plasmas **4**, 1297 (1997).
[35] E. V. Belova, R. C. Davidson, H. Ji, M. Yamada, C. D. Cothran, M. R. Brown, and M. J. Schaffer, Nucl. Fusion **46**, 162 (2006).

[36]E. N. Parker, J. Geophys. Res. **62**, 509 (1957).
[37]R. D. Milroy and J. U. Brackbill, Phys. Fluids **29**, 1184 (1986).
[38]L. C. Steinhauer and A. Ishida, Phys. Rev. Lett. **79**, 3423 (1997).
[39]L. C. Steinhauer and A. Ishida, Phys. Plasmas **5**, 2609 (1998).
[40]Z. Yoshida and S. M. Mahajan, Phys. Rev. Lett. **88**, 095001 (2002).
[41]F. Glass, B. H. Deng, E. Garate, O. Gornostaeva, and J. Schroeder, Rev. Sci. Instrum. **81**, 10D506 (2010).
[42]Y. Ono, M. Yamada, T. Akao, T. Tajima, and R. Matsumoto , Phys. Rev. Lett. **76**, 3328 (1996).
[43]D. K. Gupta, E. Paganini, A. Balvis, L. Bonell, B. H. Deng, F. Giammanco, O. Gornostaeva, R. Hayashi, K. Knapp, P. Marsili, M. McKenzie, R. Pousa-Hijos, S. Primavera, J. Schroeder, and M. Tuszewski, Rev. Sci. Instrum. **81**, 10D737 (2010).
[44]P. C. Stangeby, *The Plasma Boundary of Magnetic Fusion Devices* (Taylor & Francis Group, London, 2000)
[45]Yu. A. Omelchenko, Phys. Plasmas **7**, 1443 (2000).
[46]K. Wira and Z. A. Pietrzyk, Phys. Fluids B **2**, 561 (1990).
[47]R. D. Milroy and L. C. Steinhauer, Phys. Plasmas **15**, 022508 (2008).
[48]E. V. Belova, R. C. Davidson, H. Ji, and M. Yamada, Phys. Plasmas **11**, 2523 (2004).
[49]E. V. Belova, R. C. Davidson, H. Ji, and M. Yamada, Phys. Plasmas **13**, 056115 (2006).
[50]S. Ohi, T. Minato, Y. Kawakami, M. Tanjyo, S. Okada, Y. Ito, M. Kako, S. Gotô, T. Ishimura, and H. Itô, Phys. Rev. Lett. **51**, 1042 (1983).
[51]T. Ishimura, Phys. Fluids **27**, 2139 (1984).
[52]R. E. Siemon, W. T. Armstrong, D. C. Barnes, R. R. Bartsch, R. E. Chrien, J. C. Cochrane, W. N. Hugrass, R. W. Kewish, Jr., P. L. Klingner, H. R. Lewis, R. K. Linford, K. F. McKenna, R. D. Milroy, D. J. Rej, J. L. Schwarzmeier, C. E. Seyler, E. G. Sherwood, R. L. Spencer, and M. Tuszewski, Fusion Technol. **9**, 13 (1986).
[53]L. C. Steinhauer, Phys. Fluids B **4**, 4012 (1992).
[54]J. Wesson, *Tokamaks* (Clarendon Press, Oxford, 2004).